

# Joint Oscillation Damping and Inertia Provision Service for Converter-Interfaced Generation

Cheng Feng, *Student Member, IEEE*, Linbin Huang, *Member, IEEE*, Xiuqiang He, *Member, IEEE*, Yi Wang, *Member, IEEE*, Florian Dörfler, *Senior Member, IEEE*, Qixin Chen, *Senior Member, IEEE*,

**Abstract**—As renewable generation becomes more prevalent, traditional power systems dominated by synchronous generators are transitioning to systems dominated by converter-interfaced generation. These devices, with their weaker damping capabilities and lower inertia, compromise the system’s ability to withstand disturbances, pose a threat to system stability, and lead to oscillations and poor frequency response performance. While some new converter-interfaced generations are capable of providing superior damping and fast frequency control, there is a lack of effective measures to incentivize manufacturers to adopt them. To address this gap, this paper defines the joint oscillation damping and inertia provision services at the system level, seeking to encourage converter-interfaced generation to provide enhanced damping and fast frequency response capabilities. Our approach is anchored in a novel convex parametric formulation that combines oscillation mode and frequency stability constraints. These constraints ensure a sufficient damping ratio for all oscillation modes and maintain transient frequency trajectories within acceptable limits. They are designed to integrate smoothly into various operational and planning optimization frameworks. Using this formulation, we introduce a joint service for oscillation damping and inertia provision based on a cost-minimization problem. This facilitates the optimal allocation of damping and virtual inertia to converters, achieving both small-signal stability and frequency stability. Furthermore, we investigate the economic effects of introducing this service into a new ancillary service market, assessing its impact on system operations and cost-efficiency. Numerical tests highlight the service’s efficacy in ensuring both small-signal stability and frequency stability, and offer insights into potential economic benefits.

**Index Terms**—Power system stability, converter-interfaced generation, oscillation damping, virtual inertia, frequency stability, ancillary service.

## I. INTRODUCTION

The electric power system is currently undergoing a profound transformation, with an increasing share of renewable generation sources connecting to the grid via power electronic converters. This shift towards systems dominated by converter-interfaced generation has generally resulted in lower inertia and weakened damping [1], [2]. This reduces the ability of the system to resist disturbances. It becomes more challenging for the system to react with fast frequency response, and to dampen an oscillation component swiftly and sufficiently, thereby escalating the risk of sustained and severe oscillations which could jeopardize the safety of the system operation [3].

To maintain system stability and mitigate oscillations with a high penetration of converters, various research initiatives are undergoing to design advanced converter controllers. These efforts aim to improve existing grid-following converters [4], as well as pioneer new grid-forming control structures [5]. These improvements are designed to support stable grid oper-

ation, including but not limited to offering superior damping capabilities and virtual inertia to the network [6]. Currently, since the contribution of converters to system stability is not adequately rewarded, there is a lack of an effective incentive that encourages converter manufacturers to adopt these new structures. Therefore, it becomes critical to establish a new service to incentivize the deployment of high-performing converters by rewarding the provision of oscillation damping and virtual inertia. It should be noted that instabilities often arise from interactions between individual generator units and the overall network [3], [7]. Therefore, a configuration that is not deliberately designed might not effectively damp oscillations and improve frequency response performances [8]. As such, it is necessary for system operators to perform system-wide optimizations to place damping and inertia [9].

Incorporating stability constraints into operational problems is a critical concern and has been demonstrated to be an important measure to ensure stability [10]. During the era of systems dominated by synchronous machines, researchers explored ways to include transient stability [11], [12] and voltage stability constraints [13] into operational and optimal power flow models. These studies aimed to determine the limits of transient transmission power [11], [12], or iteratively redispatching power generators to keep the system stable [14]. The integration of converter-interfaced generation sparked additional research about this topic. From the perspective of frequency stability, Ref. [15] investigated the cost-efficient provision of inertia and fast frequency reserves from converters to improve transient performance. Ref. [16] further highlighted the differences in inertia provision between grid-following and grid-forming converters, and suggested strategic placement of inertia to enhance key dynamic performance metrics. Regarding the stability service market, recent research focused on designing virtual inertia provision services either by organizing a standalone new service [17] or by integrating it into the energy service [18]. Much of the existing literature primarily emphasized the frequency stability while overlooked variations in frequency oscillations between nodes and areas.

Moreover, a growing body of work suggests that, in systems with a high penetration of converter-interfaced generation, small-signal stability is of significant concern [1], and damping plays a more pivotal role than inertia [19], [20]. Some research explored the spacial configuration of converter damping across different units to improve the small-signal performance. In the planning phase, Ref. [21] suggested the optimal placing of damping-enhanced converters can effectively improve grid strength and therefore small-signal stability. During real-time operations, Ref. [22], [23] attempted to directly adjust the

damping coefficients of converters to achieve optimal performance. To achieve this, existing research typically built a non-convex model to configure the oscillation damping. They employed sensitivity factors of oscillation modes to adjust modal damping ratio iteratively, resulting in significant complexity in iterations. Some research has aimed to analytically calculate oscillation modes [24], [25] or time-domain responses [19], [26]. These efforts assume that all units have equal inertia-to-damping ratios. The limitations due to the non-convex problems or the uniform inertia-damping assumption present significant challenges in incorporating these methods into system operations, which hinders the development of the oscillation damping service.

To summarize, for the first time, this paper proposes the establishment of the *joint oscillation damping and inertia provision service* for converter-interfaced generation, ensuring both small-signal stability and frequency stability simultaneously. The service is built upon a convex model, eliminating the need for complex iterations or uniform inertia-damping assumption. The primary contributions are as follows:

- Formulate convex constraints to enforce satisfactory oscillation damping and fast frequency response performance. These constraints are designed for direct integration into various operational and planning optimization frameworks for broader applicability.
- Develop the joint oscillation damping and inertia provision service using a convex cost minimization framework to place damping and virtual inertia throughout the network. The model ensures a broader type of stability while achieving cost-efficiency in acquiring damping and inertia.
- Investigate the effects of assimilating the joint oscillation damping and inertia provision service into the ancillary service markets. Numerical results demonstrate the effectiveness of the proposed service in ensuring system stability and enhancing cost efficiencies.

In Section II, the service setup is explained and the transient models for different types of generation units are provided. The section also elaborates on the convex small-signal constraints and frequency stability constraints related to damping and virtual inertia. In Section III, we analyze the stability-related costs of converters, and present the complete cost minimization model for allocating damping and inertia. This section also details the incorporation of the novel service within the ancillary service market. Section IV offers numerical validation of the proposed service and its economic implications. Conclusions are provided in Section V.

*Notation:* The following conventions are used in this paper: Scalars are represented in normal font. Vectors (column vectors by default) are represented in bold italics. Matrices are represented in bold upright font.  $\mathbf{0}$  represents a zero matrix/vector,  $\mathbf{I}$  indicates the identity matrix, and  $\mathbf{1}$  denotes an all-one vector, all of which are with proper dimension. Transpose of a vector/matrix is represented by  $\mathbf{x}^\top$ . Conjugate of a scalar/vector/matrix is represented by  $\mathbf{x}^*$ . Conjugate transpose of a vector/matrix is represented by  $\mathbf{x}^H$ . The inner product  $\mathbf{x}$  and  $\mathbf{y}$  is denoted as  $\langle \mathbf{x}, \mathbf{y} \rangle = \mathbf{x}^H \mathbf{y}$ .  $h(s)$  refers to the Laplace domain representation of a function  $h(t)$ , while the latter refers

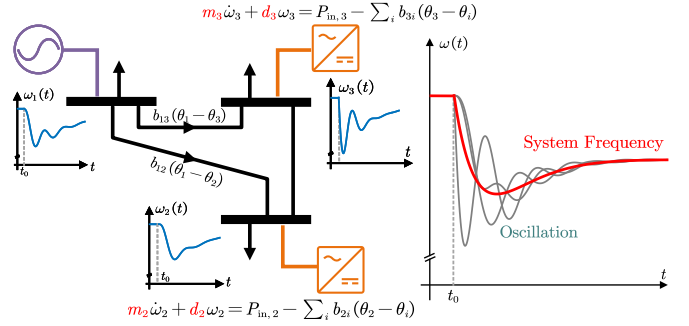


Fig. 1. The joint oscillation damping and inertia provision service aims to mitigate oscillations and improve poor frequency performances via procuring nodal damping  $d$  and virtual inertia  $m$  from different units.

to its time domain representation.  $\|x(t)\|_\infty = \max_t |x(t)|$  represents the  $\mathcal{L}_\infty$  norm.

## II. SERVICE SETTING AND STABILITY CONSTRAINTS

### A. Setting and System Model

The primary goal of the power system operator is to maintain system stability, ensuring that, even after significant disturbances, transient response performance remains within acceptable limits. It is crucial to ensure that the damping and inertia levels at different nodes can effectively mitigate the adverse effects of disturbances, including inter-area oscillations and poor frequency response performances. Consequently, system operators are turning to converters to procure damping and virtual inertia as a new ancillary service. For simplicity, this study proposes a separate ancillary service to acquire inertia and damping independently from the energy service. Notably, the optimization problem presented in this study is formulated as a convex optimization problem, facilitating its integration with the unit commitment and optimal power flow model for co-clearing the energy service.

Consider a converter-dominated system, as depicted in Fig.1, where generation units are connected via a lossless transmission grid. In this setup, the buses are represented by the set  $\mathcal{N} = \{1, \dots, i, \dots, I\}$ . The set of buses,  $\mathcal{N}$ , is partitioned into  $\mathcal{N}_G$  and  $\mathcal{N}_L$ . Specifically,  $\mathcal{N}_G$  denotes the set of buses connected to generation units (if any), while  $\mathcal{N}_L$  refers to those connected exclusively to loads. The generation units belong to the set  $\mathcal{G}$ , defined as  $\mathcal{G} = \{1, \dots, k, \dots, K\}$ , which is partitioned into  $\mathcal{G}_C$  and  $\mathcal{G}_G$ .  $\mathcal{G}_C$  denotes the set of converter-interfaced generation units, while  $\mathcal{G}_G$  refers to the set of synchronous generators. The angle and frequency dynamics for converter-interfaced generation unit  $k \in \mathcal{G}_C$  are as follows:

$$\dot{\theta}_k = \omega_k \quad (1)$$

$$m_k \dot{\omega}_k + d_k \omega_k = P_{in,k} - \sum_{i=1}^{i=I} b_{ki} (\theta_k - \theta_i) \quad (2)$$

With a slight deviation from strict notation, all state variables represent deviations from their nominal values. In the model above,  $\theta_k, \omega_k$  represent the phase angle and frequency at its terminal bus;  $m_k, d_k$  denote its virtual inertia and damping coefficient;  $P_{in,k}$  denotes the net power injection; and  $b_{ki}$  denotes the line inductance between generation  $k$  and its

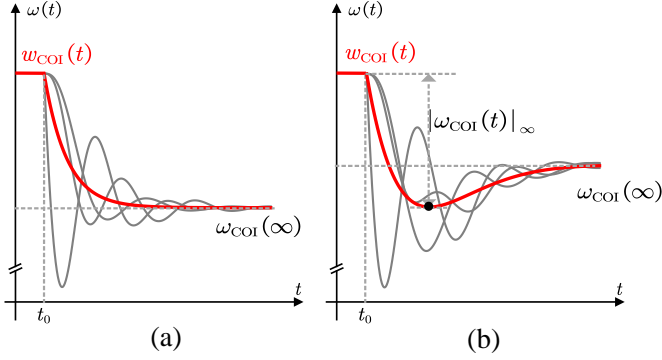


Fig. 2. (a) Nodal and center of inertia (COI) frequency trajectories without turbine dynamics. (b) Nodal and center of inertia (COI) frequency trajectories with turbine dynamics.

neighboring bus  $i$ . We presume voltage magnitude is fixed. Using DC power flow, the term  $b_{ki}(\theta_k - \theta_i)$  represents the flow on the line between generation unit  $k$  and its neighboring bus  $i$ . The converter-interfaced generations can adjust their damping coefficients  $d_k$  and virtual inertia  $m_k$  flexibly. The system operator can treat them as optimizable variables and procure an adequate amount of damping and virtual inertia from converters to improve system stability.

The angle and frequency dynamics for synchronous generators  $k \in \mathcal{G}_G$  are as follows:

$$\dot{\theta}_k = \omega_k \quad (3)$$

$$m_k \dot{\omega}_k = P_{in,k} + P_{u,k} - \sum_{i=1}^{i=I} b_{ki}(\theta_k - \theta_i) \quad (4)$$

$$\tau_k \dot{P}_{u,k} = -P_{u,k} - r_k^{-1} \omega_k \quad (5)$$

where  $r_k$  is the frequency-power droop regulation constant,  $\tau_k$  is the turbine time constant, and  $m_k$  denotes its rotational inertia. Synchronous generators cannot adjust their inertia, so they are treated as fixed parameters. Besides, the generator and load damping is small compared to that of converter-interfaced generation units, and thus it is neglected.

### B. Oscillation Damping Constraints

The turbine dynamics (5) inject power in proportion to the frequency droop  $r_k$ . However, due to the inherent mechanical processes and the associated power ramping delays  $\tau_k$ , their response is not instantaneous. As shown in Fig.2(b), the response lags by  $\tau_k$  in comparison to the immediate damping. Consequently, the turbine dynamics generally do not contribute to oscillation damping and are thus neglected when assessing their oscillation damping effects. Thereby, the state-space model of (1)-(4) is represented as:

$$\begin{bmatrix} \dot{\theta} \\ \dot{\omega} \end{bmatrix} = \begin{bmatrix} \mathbf{0} & \mathbf{I} \\ -\mathbf{M}^{-1}\mathbf{L} & -\mathbf{M}^{-1}\mathbf{D} \end{bmatrix} \begin{bmatrix} \theta \\ \omega \end{bmatrix} + \begin{bmatrix} \mathbf{0} \\ -\mathbf{M}^{-1} \end{bmatrix} \mathbf{P}_{dis} \quad (6)$$

where  $\mathbf{L} = \mathbf{L}_{\mathcal{N}_G, \mathcal{N}_G} - \mathbf{L}_{\mathcal{N}_G, \mathcal{N}_L} \mathbf{L}_{\mathcal{N}_L, \mathcal{N}_L}^{-1} \mathbf{L}_{\mathcal{N}_L, \mathcal{N}_G}$  represents the nodal admittance matrix after eliminating the load node  $\mathcal{N}_L$  through Kron reduction [27].  $\mathbf{P}_{dis} = \mathbf{P}_{dis, \mathcal{N}_G} + \mathbf{L}_{\mathcal{N}_G, \mathcal{N}_L} \mathbf{L}_{\mathcal{N}_L, \mathcal{N}_L}^{-1} \mathbf{P}_{dis, \mathcal{N}_L}$  denotes the disturbance at node  $i$  after redistribution by the power network.  $\mathbf{M} = \text{diag}(m_i) \succ$

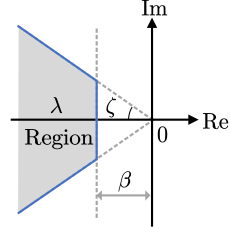


Fig. 3. The desired location region of the dominant oscillation mode  $\lambda$  in the complex plane.

$\mathbf{0}$ ,  $\mathbf{D} = \text{diag}(d_i) \succcurlyeq \mathbf{0}$  are the diagonal matrices representing aggregated nodal inertia and damping coefficients of all the generation units at node  $i$ , respectively. This paper allows multiple generation units locate at one node. In that case, the nodal inertia  $m_i$  and damping  $d_i$  are the sum of inertia  $m_k$  and damping  $d_k$  from individual units located at node  $i$ .

The objective of the oscillation damping constraints is to ensure that the system's dominant oscillation mode, denoted as  $\lambda \in \mathbb{C}$ , falls within the region depicted in Fig.3. This designated region encompasses a plane defined by  $\text{Re}(\lambda) \leq -\beta$  and a conical area represented by the equation  $\sin \zeta \cdot \text{Re}(\lambda) + \cos \zeta \cdot \text{Im}(\lambda) \leq 0$ . These constraints ensure that all system modes exhibit sufficient decay speed  $\beta$  and maintain a low oscillation damping ratio  $\zeta$ .

The oscillation modes  $\lambda$  are the eigenvalues of the state matrix of (6). The eigenvalue  $\lambda$  and its eigenvector  $[\boldsymbol{\nu}^T \boldsymbol{\xi}^T]^T$  satisfy the following condition:

$$\begin{bmatrix} \mathbf{0} & \mathbf{I} \\ -\mathbf{M}^{-1}\mathbf{L} & -\mathbf{M}^{-1}\mathbf{D} \end{bmatrix} \begin{bmatrix} \boldsymbol{\nu} \\ \boldsymbol{\xi} \end{bmatrix} = \lambda \begin{bmatrix} \boldsymbol{\nu} \\ \boldsymbol{\xi} \end{bmatrix} \quad (7)$$

which can be equivalently expressed as:

$$\boldsymbol{\xi} = \lambda \boldsymbol{\nu}, \quad -\mathbf{L}\boldsymbol{\nu} - \mathbf{D}\boldsymbol{\xi} = \lambda \mathbf{M}\boldsymbol{\xi} \quad (8)$$

Replacing  $\boldsymbol{\xi}$  in the second equation in Eqs.(8) via the first equation, we get

$$\lambda^2 \mathbf{M}\boldsymbol{\nu} + \lambda \mathbf{D}\boldsymbol{\nu} + \mathbf{L}\boldsymbol{\nu} = \mathbf{0} \quad (9)$$

The solution to finding  $\lambda$  for Eq.(9) is known as the quadratic eigenvalue problem (QEP) [28]. QEP is widely used in other fields, such as dynamic acoustics analysis and fluid mechanics. Usually, sophisticated algorithms are employed to solve the problem numerically. By multiplying both sides of Eq.(9) with the conjugate transpose of eigenvector  $\boldsymbol{\nu}^H$ , we can transform it into a scalar quadratic equation concerning  $\lambda$ :

$$\lambda^2 \langle \boldsymbol{\nu}, \mathbf{M}\boldsymbol{\nu} \rangle + \lambda \langle \boldsymbol{\nu}, \mathbf{D}\boldsymbol{\nu} \rangle + \langle \boldsymbol{\nu}, \mathbf{L}\boldsymbol{\nu} \rangle = 0 \quad (10)$$

If the discriminant  $\langle \boldsymbol{\nu}, \mathbf{D}\boldsymbol{\nu} \rangle^2 - 4 \langle \boldsymbol{\nu}, \mathbf{M}\boldsymbol{\nu} \rangle \langle \boldsymbol{\nu}, \mathbf{L}\boldsymbol{\nu} \rangle$  is non-negative, it results in two real roots. Among them, one serves as an eigenvalue to (6). On the other hand, a negative discriminant implies the presence of a pair of conjugate complex eigenvalues. Notably, zero is an eigenvalue of the system. This is inherently attributed to the eigenvalue of the admittance matrix, as elaborated below:

*Property 1* (Laplacian Matrix [27]).  $\mathbf{L}$  is positive semi-definite and with eigenvalue 0 whose eigenvector is  $\mathbf{1}$ .

*Lemma 1* (0 Eigenvalue). 0 is an eigenvalue of (6) and the corresponding eigenvector is  $[\mathbf{v}^\top \ \boldsymbol{\xi}^\top]^\top = [\mathbf{1}^\top \ \mathbf{0}^\top]^\top$ .

The eigenvalue of 0 represents a global shift in the phase angles of all the generation units, signifying the absence of a fixed reference point for phase angles.

1) *Oscillation Mode Decay*: The distance of an eigenvalue to the imaginary axis determines the decaying speed. Therefore, the location constraint  $\text{Re}(\lambda) \leq -\beta$  is essential as it ensures that transient fluctuations in angles and frequencies do not persist over an extended period. Consider the right-shifting version of the eigenvalue solution of Eq.(10):

$$\begin{aligned} & (\hat{\lambda} - \beta)^2 \mathbf{M}\boldsymbol{\nu} + (\hat{\lambda} - \beta) \mathbf{D}\boldsymbol{\nu} + \mathbf{L}\boldsymbol{\nu} \\ & = \hat{\lambda}^2 \mathbf{M}\boldsymbol{\nu} + \hat{\lambda} (\mathbf{D} - 2\beta \mathbf{M}) \boldsymbol{\nu} + (\mathbf{L} - \beta \mathbf{D} + \beta^2 \mathbf{M}) \boldsymbol{\nu} = \mathbf{0} \end{aligned} \quad (11)$$

where  $\hat{\lambda} = \lambda + \beta$  is the solution to the shifted problem Eq.(11) when  $\lambda$  is the solution to Eq.(10). In a scenario where all the eigenvalues of the shifted system (excluding the eigenvalue  $0 + \beta$ , cf. Lemma 1) lie in the left half plane, the dominant pole of the original system will reside in the plane  $\text{Re}(\lambda) \leq -\beta$ . The following proposition elaborates on how to constrain the eigenvalues to lie within the plane  $\text{Re}(\lambda) \leq -\beta$  using the shifted problem outlined in Eq.(11):

*Proposition 1* (Mode Decay). The eigenvalues of (6) will all be within  $\text{Re}(\lambda) \leq -\beta$  except for eigenvalue 0 if exists a positive variable  $v$  so that:

$$\mathbf{D} - 2\beta \mathbf{M} \succcurlyeq \mathbf{0} \quad (12)$$

$$\mathbf{L} - \beta \mathbf{D} + \beta^2 \mathbf{M} + v \mathbf{1}\mathbf{1}^\top \succcurlyeq \mathbf{0} \quad (13)$$

*Proof*. See appendix.  $\square$

*Remark*. The constraints are convex with respect to  $\mathbf{M}$ ,  $\mathbf{D}$ , and  $\mathbf{L}$ . In the service, the system operator cares about optimizing  $\mathbf{M}$  and  $\mathbf{D}$ . Meanwhile, these constraints can be incorporated into problems that can change the network topology  $\mathbf{L}$ . This includes applications like power network planning and controls for switching high-voltage direct current transmission lines.

2) *Mode Damping Ratio*: The angle  $\zeta$  between the vector connecting complex plane origin to the eigenvalue and the real axis yields the oscillation damping ratio. A larger oscillation damping angle  $\zeta$  corresponds to more severe oscillation. The constraint in the conic region,  $\sin \zeta \cdot \text{Re}(\lambda) + \cos \zeta \cdot \text{Im}(\lambda) \leq 0$ , ensures that the system does not undergo serious oscillation. The following lemma provides the condition under which an eigenvalue  $\lambda$  lies within the desired conic region, a condition typically referred to as the  $\mathcal{D}$ -stability criterion [29]:

*Lemma 2* (Conic Region [29]). The eigenvalue  $\lambda$  is in the conic region  $\sin \zeta \cdot \text{Re}(\lambda) + \cos \zeta \cdot \text{Im}(\lambda) \leq 0$  if and only if the following condition is satisfied:

$$\sin \zeta \cdot (\lambda + \lambda^*) \leq 0 \quad (14)$$

$$(\sin \zeta)^2 (\lambda + \lambda^*)^2 + (\cos \zeta)^2 (\lambda - \lambda^*)^2 \geq 0 \quad (15)$$

where  $\lambda^*$  is the conjugate of the complex eigenvalue  $\lambda$ .

Eq.(14) constrains the real part of the eigenvalue to be negative, while Eq.(15) ensures the ratio between the imaginary and real parts falls within the desired range. Leveraging

the relationship between coefficients and roots, Lemma 2 can be transformed into a requirement for the coefficients of the eigenvalue solution problem in Eq.(10):

*Proposition 2* (Mode Damping). All the eigenvalues lie in the conic region  $\sin \zeta \cdot \text{Re}(\lambda) + \cos \zeta \cdot \text{Im}(\lambda) \leq 0$  if and only if the following condition is satisfied:

$$\langle \boldsymbol{\nu}, \mathbf{D}\boldsymbol{\nu} \rangle^2 - 4 (\cos \zeta)^2 \langle \boldsymbol{\nu}, \mathbf{L}\boldsymbol{\nu} \rangle \langle \boldsymbol{\nu}, \mathbf{M}\boldsymbol{\nu} \rangle \geq 0 \quad (16)$$

*Proof*. See appendix.  $\square$

*Remark*. Proposition 2 indicates that increasing the nodal inertia might lead to unanticipated inter-area oscillations. Thus, the virtual inertia does not necessarily promote small-signal stability in a ‘monotonic’ fashion.

3) *Summary*: Proposition 2 provides a necessary and sufficient condition to ensure all the eigenvalues are situated in the desired conic region. The constraint in Eq.(16) is non-convex because it also depends on the eigenvectors. However, the mode decay constraint Eq.(12) provides a natural method for transforming the the constraint Eq.(16) into a convex constraint. With the constraint Eq.(12), it is ensured that  $\langle \boldsymbol{\nu}, \mathbf{D}\boldsymbol{\nu} \rangle \geq 2\beta \langle \boldsymbol{\nu}, \mathbf{M}\boldsymbol{\nu} \rangle$ . As a result,  $\langle \boldsymbol{\nu}, \mathbf{D}\boldsymbol{\nu} \rangle^2 \geq 2\beta \langle \boldsymbol{\nu}, \mathbf{M}\boldsymbol{\nu} \rangle \langle \boldsymbol{\nu}, \mathbf{D}\boldsymbol{\nu} \rangle$ . Therefore, by combining Proposition 1 and Proposition 2, we obtain the convex constraints needed to constrain the poles in the desired region as follows:

*Theorem 1* (Mode Placement Constraints). If the following condition is satisfied, all the eigenvalues are in the left plane  $\lambda \leq -\beta$  and the conic region  $\sin \zeta \cdot \text{Re}(\lambda) + \cos \zeta \cdot \text{Im}(\lambda) \leq 0$  simultaneously:

$$(12) - (13), \quad \beta \mathbf{D} - 2 (\cos \zeta)^2 \mathbf{L} \succcurlyeq \mathbf{0} \quad (17)$$

*Proof*. See appendix.  $\square$

*Remark*. When constraint Eq.(12) is strictly binding ( $\mathbf{D} = 2\beta \mathbf{M}$ ), all nodes in the system adopt the uniform inertia/damping ratio  $2\beta$ . The oscillation modes can be directly computed, as indicated by extensive research [19], [24], [26]. However, Theorem 1 does not necessitate a uniform inertia/damping ratio assumption. These constraints may be regarded as a robust set that constrains the system modes without the need for explicit calculation of the exact eigenvalues.

*Remark*. Proposition 1 and Theorem 1 provide the sufficient but not necessary parametric conditions to constrain the location of eigenvalues. The necessary and sufficient conditions to place eigenvalues can be obtained via linear matrix inequalities (LMIs, see Ref. [30] Chapter 3.2). However, for this case, the LMI conditions turn out to be non-convex bi-linear matrix inequalities. The proposed constraints are convex but can be more conservative than the ‘LMI’ approach.

### C. Frequency Stability Constraints

1) *Global Frequency Coordinate*: Frequency stability is concerned with the global frequency response to disturbances. Common indicators of frequency stability performance in the system include the rate of change of frequency (RoCoF), frequency nadir, and the steady-state frequency under the center of inertia (COI) coordinate subsequent to a significant

step disturbance. Typically, when slower dynamics, such as those of the generator turbine (5), are factored in, a nadir in the COI frequency becomes evident, as shown in Fig.2(b). Keeping in line with traditional methodology, we can delineate the dynamics including a turbine in the COI coordinate as follows [31], [32]:

$$m_\Sigma \dot{\omega}_{\text{COI}} + d_\Sigma \omega_{\text{COI}} = P_\Sigma + P_u \quad (18)$$

$$\tau \dot{P}_u = -P_u - r^{-1} \omega_{\text{COI}} \quad (19)$$

where  $m_\Sigma = \mathbf{1}^\top \mathbf{M} \mathbf{1}$ ,  $d_\Sigma = \mathbf{1}^\top \mathbf{D} \mathbf{1}$  and  $P_\Sigma = \mathbf{1}^\top \mathbf{P}_{\text{dis}}$  represent the total inertia, total damping, and total disturbance of the system, respectively. It has been established that the aggregated turbine dynamics of  $r$  and  $\tau$  are independent of  $m_\Sigma$  and  $d_\Sigma$  [31], [32]. Consequently, they can be treated as fixed parameters rather than variables.

In the subsequent analysis, we mainly consider the disturbance as a step input  $s^{-1} p_\Sigma$ , where  $p_\Sigma$  denotes the magnitude of the disturbance. According to Eqs.(18)-(19),  $\omega_{\text{COI}}(s)$  can be represented as:

$$\omega_{\text{COI}}(s) = \frac{p_\Sigma (\tau s + 1)}{s (m_\Sigma \tau s^2 + (m_\Sigma + d_\Sigma \tau) s + d_\Sigma + r^{-1})} \quad (20)$$

2) *Rate of Change of Frequency (RoCoF)*: The maximum RoCoF is obtained at the time instant  $t = 0^+$  [31]. The RoCoF at the time instant  $t = 0^+$  can be obtained via the initial value theorem as follows:

$$|\dot{\omega}_{\text{COI}}(t)|_\infty = \lim_{s \rightarrow \infty} s \cdot \dot{\omega}_{\text{COI}}(s) = m_\Sigma^{-1} |p_\Sigma| \quad (21)$$

The RoCoF should be below  $\varepsilon_{\text{RoCoF}}$ , so the constraint can be represented by:

$$|p_\Sigma| \leq \varepsilon_{\text{RoCoF}} m_\Sigma \quad (22)$$

3) *Steady State Frequency*: The system will stabilize to a synchronized frequency, as shown in Fig.2(b). The steady-state frequency deviations can be obtained via the final value theorem:

$$|\omega_{\text{COI}}(\infty)| = \lim_{s \rightarrow 0} s \cdot \omega_{\text{COI}}(s) = (d_\Sigma + r^{-1})^{-1} |p_\Sigma| \quad (23)$$

If the maximum allowed steady-state frequency deviation is  $\varepsilon_{\text{sync}}$ , then the constraint can be expressed as follows:

$$|p_\Sigma| \leq \varepsilon_{\text{sync}} (d_\Sigma + r^{-1}) \quad (24)$$

where the right-hand side of (24) is normally used to define droop slopes of the system.

4) *Frequency Nadir*: The time-domain representation of  $\omega_{\text{COI}}(t)$  can be derived by executing the inverse Laplace transform on Eq.(20). By setting  $\dot{\omega}_{\text{COI}}(t) = 0$ , we can determine the time of the frequency nadir and subsequently derive the expressions for the frequency nadir.

*Lemma 3* (Frequency Nadir [31]). Given the power system COI frequency dynamics via Eq.(20), if the system is underdamped, the COI frequency nadir of the system frequency  $|\omega_{\text{COI}}|$  is given by:

$$|\omega_{\text{COI}}(t)|_\infty = \frac{|p_\Sigma|}{d_\Sigma + r^{-1}} \left( 1 + \sqrt{\frac{\tau r^{-1}}{m_\Sigma}} e^{-\frac{\eta}{\omega_d} (\phi + \frac{\pi}{2})} \right) \quad (25)$$

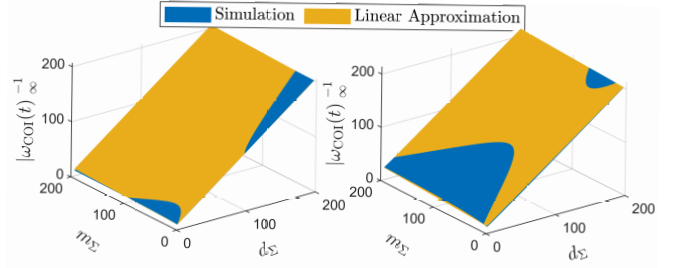


Fig. 4. Simulated and linear approximated  $|\omega_{\text{COI}}|_\infty^{-1}$  under unit step disturbance. Left: Slow ( $\tau = 10$ ) and light ( $r^{-1} = 5$ ) turbine dynamics ( $\kappa = 20$ ). Right: Fast ( $\tau = 5$ ) and strong ( $r^{-1} = 20$ ) turbine dynamics ( $\kappa = 10$ ).

where  $\omega_d$ ,  $\eta$ , and  $\phi$  are uniquely determined by:

$$\omega_d = \sqrt{\frac{d_\Sigma + r^{-1}}{m_\Sigma \tau} - \frac{1}{4} \left( \frac{1}{\tau} + \frac{d_\Sigma}{m_\Sigma} \right)^2}, \quad \eta = \frac{1}{2} \left( \tau^{-1} + \frac{d_\Sigma}{m_\Sigma} \right)$$

$$\sin(\phi) = \frac{(\tau^{-1} - \eta)}{\sqrt{\omega_d^2 + (\tau^{-1} - \eta)^2}} = \frac{m_\Sigma - d_\Sigma \tau}{2\sqrt{m_\Sigma \tau r^{-1}}}$$

Direct attempts to constrain the frequency nadir using Eq.(25) result in a formulation that is highly non-convex. By undertaking a numerical analysis concerning the partial derivatives of Eq.(25) with respect to  $m_\Sigma$  and  $d_\Sigma$ , the subsequent numerical findings are generally observed:

$$\frac{\partial^2 |\omega_{\text{COI}}(t)|_\infty^{-1}}{\partial (m_\Sigma)^2} \approx 0, \quad \frac{\partial^2 |\omega_{\text{COI}}(t)|_\infty^{-1}}{\partial (d_\Sigma)^2} \approx 0, \quad \frac{\partial^2 |\omega_{\text{COI}}(t)|_\infty^{-1}}{\partial m_\Sigma \partial d_\Sigma} \approx 0$$

This implies that  $|\omega_{\text{COI}}(t)|_\infty^{-1}$  can be reasonably approximated using a linear function with respect to  $m_\Sigma$  and  $d_\Sigma$ , provided that neither  $m_\Sigma$  nor  $d_\Sigma$  is exceptionally large. Numerical tests confirm this observation within typical ranges of  $m_\Sigma$  and  $d_\Sigma$ . The next task is to derive the specific linear expression that approximates  $|\omega_{\text{COI}}(t)|_\infty^{-1}$ .

With  $r$  and  $\tau$  fixed, we can define the following function of  $m_\Sigma$  and  $d_\Sigma$ , representing the inverse of the frequency nadir as described in (25) for a unit disturbance scenario:

$$\mathcal{H}(m_\Sigma, d_\Sigma) := \left( \frac{1}{d_\Sigma + r^{-1}} \left( 1 + \sqrt{\frac{\tau r^{-1}}{m_\Sigma}} e^{-\frac{\eta}{\omega_d} (\phi + \frac{\pi}{2})} \right) \right)^{-1} \quad (26)$$

To approximate  $\mathcal{H}(m_\Sigma, d_\Sigma)$  linearly, an initial step is to identify three non-collinear points  $(m_\Sigma, d_\Sigma, \mathcal{H}(m_\Sigma, d_\Sigma))$  that satisfy the relationship given in (26). Using these points, one can construct a potential linear approximation for  $\mathcal{H}(m_\Sigma, d_\Sigma)$ . This study utilizes the triad:  $(r^{-1}, r^{-1}, \mathcal{H}(r^{-1}, r^{-1}))$ ,  $(r^{-1}, \kappa r^{-1}, \mathcal{H}(r^{-1}, \kappa r^{-1}))$ , and  $(\kappa r^{-1}, r^{-1}, \mathcal{H}(\kappa r^{-1}, r^{-1}))$ , with  $\kappa > 1$ . The choice of the first point is to ensure proximity to the origin. The parameter  $\kappa$  is adjusted so that the latter two points are distinctly spaced from the first and closely aligned with the typical boundaries for  $m_\Sigma$  and  $d_\Sigma$ . This selection ensures the approximation is representative over extensive ranges of  $m_\Sigma$  and  $d_\Sigma$ . Fig.4 showcases two examples of these linear approximations. The

outcomes from both the simulation and the linear approximation formula align so closely that their plots nearly coincide.

Suppose we approximate the relationship between  $m_\Sigma$ ,  $d_\Sigma$ , and  $\mathcal{H}(m_\Sigma, d_\Sigma)$  linearly, as derived from the method described above. This relationship can be expressed as:

$$\mathcal{H}(m_\Sigma, d_\Sigma) = \Theta_d d_\Sigma + \Theta_m m_\Sigma + \Theta \quad (27)$$

Here,  $\Theta_d$ ,  $\Theta_m$ , and  $\Theta$  are constant coefficients determined by the three selected points:

$$\begin{aligned} \Theta_m &= r (\mathcal{H}(\kappa r^{-1}, r^{-1}) - \mathcal{H}(r^{-1}, r^{-1})) / (\kappa - 1) \\ \Theta_d &= r (\mathcal{H}(r^{-1}, \kappa r^{-1}) - \mathcal{H}(r^{-1}, r^{-1})) / (\kappa - 1) \\ \Theta &= -\Theta_m r^{-1} - \Theta_d r^{-1} + \mathcal{H}(r^{-1}, r^{-1}) \end{aligned} \quad (28)$$

Now, given a threshold for post-disturbance frequency nadir,  $\varepsilon_{\text{nadir}}$ , we can express the relevant constraint as:

$$|p_\Sigma| \leq \varepsilon_{\text{nadir}} (\Theta_d d_\Sigma + \Theta_m m_\Sigma + \Theta) \quad (29)$$

As the coefficients  $\Theta_d$ ,  $\Theta_m$ , and  $\Theta$  solely depend on  $r$  and  $\tau$ , they're treated as parameters. Hence, the constraint, as defined by (29), is convex with respect to both  $d_\Sigma$  and  $m_\Sigma$ .

### III. OPTIMIZATION PROBLEM FORMULATION AND SERVICE MARKET

#### A. Cost Function

1) *Reserve Power Cost*: To deal with large disturbances, converters should deviate from their maximum power tracking points and reserve the necessary power. The reserve power cost is related to the maximum output power as follows:

$$C_{k,p} = a_{k,p} \|m_k \dot{\omega}_k(t)\|_\infty + b_{k,p} \|d_k \omega_k(t)\|_\infty \quad (30)$$

where  $a_{k,p}$  and  $b_{k,p}$  represent the unit costs associated with different power reductions. The term  $\|m_k \dot{\omega}_k(t)\|_\infty$  denotes the inertia power buffer. Wind farms have rotating mechanics and can provide this inertial value  $m_k$  at a lower cost. In contrast, other generators have to reserve power  $\|m_k \dot{\omega}_k(t)\|_\infty$ . Consequently, the cost coefficients,  $a_{k,p}$  and  $b_{k,p}$ , will vary.

2) *Energy Cost*: Under substantial disturbances, batteries need to discharge a fraction of their stored energy to support the grid. The energy loss cost can be expressed as follows:

$$C_{k,e} = a_{k,e} \|m_k \omega_k(t)\|_\infty + b_{k,e} \left\| d_k \int_0^t \omega_k(\tau) d\tau \right\|_\infty \quad (31)$$

where  $a_{k,e}$ ,  $b_{k,e}$  denote unit cost coefficients for different types of energy loss. The energy  $\|m_k \omega_k(t)\|_\infty$  can be charged back automatically after the secondary frequency control returns the system frequency to the nominal value. For the second term  $\|d_k \int_0^t \omega_k(\tau) d\tau\|_\infty$ , no existing controllers will push the frequency above the nominal value to recover this part of energy. Given these different recovery characteristics, the unit costs  $a_{k,e}$ ,  $b_{k,e}$  differ.

3) *Total Individual Cost*: For an individual converter, determining its impact on system dynamics can be challenging. The system operator can provide converters with the anticipated worst-case values of  $\|\int_0^t \omega_k(\tau) d\tau\|_\infty$ ,  $\|\omega_k(t)\|_\infty$ , and  $\|\dot{\omega}_k(t)\|_\infty$  in advance. Therefore, these values will be treated as constants when a converter submits its bids. In this context, the summed cost can be expressed as a quadratic function of  $m_k$  and  $d_k$ :

$$C_k(m_k, d_k) = \varrho_{m,k} m_k^2 + \mu_{m,k} m_k + \varrho_{d,k} d_k^2 + \mu_{d,k} d_k \quad (32)$$

where  $\varrho_{m,k}$ ,  $\mu_{m,k}$  represent cost coefficients for inertia and  $\varrho_{d,k}$ ,  $\mu_{d,k}$  represent cost coefficients for damping.  $C_k(m_k, d_k)$  should be the sum of  $C_{k,p}$  and  $C_{k,e}$ . The quadratic terms are added to capture a more general case where the cost may increase with the increased provision of inertia and damping.

#### B. Complete Optimization Problem and Service Market

In summary, the complete cost minimization problem to place damping and inertia is formulated as follows:

$$\begin{aligned} \min \quad & \sum_{k \in \mathcal{G}} C_k(m_k, d_k) \\ \text{s.t.} \quad & \text{Small-Signal Stability Constraints: (17)} \\ & \text{Frequency Stability Constraints: (22), (24), (29)} \end{aligned} \quad (33)$$

The decision variables are all converters' inertial and damping coefficients and auxiliary variables  $v$  in (13). The problem (33) is a convex positive semi-definite programming model.

The complete market process for the joint oscillation damping and inertia provision service is designed as follows:

- Each converter submits its bidding for  $m_k$  and  $d_k$  as  $\mathcal{B}_k(m_k, d_k)$ , which may not necessarily reflect their actual costs  $\mathcal{C}_k(m_k, d_k)$ .
- The system operator determines the amount of  $m_k$  and  $d_k$  procured from each converter.
- The system operator pays  $q_k(\mathcal{B}_k, \mathcal{B}_{-k})$  to converter  $k$  for providing  $m_k$  and  $d_k$ , where the subscript  $-k$  denotes all the other converters excluding  $k$ .

For quadratic cost functions like Eq.(33), a converter submits parameters  $\varrho_{m,k}$ ,  $\mu_{m,k}$ ,  $\varrho_{d,k}$  and  $\mu_{d,k}$ . In real implementations, the converters can submit a block-shaped, monotonically increasing bid just like bids in the energy market. Given the payment and the bidding, converter  $k$ 's total profit is:

$$u_k(\mathcal{B}_k, \mathcal{B}_{-k}) = q_k(\mathcal{B}_k, \mathcal{B}_{-k}) - C_k(m_k, d_k) \quad (34)$$

The critical task is to determine the allocations  $m_k$ ,  $d_k$ , and the payments  $q_k$  for each converter. Typically, end-users bear the cost of ancillary services through additional fees. To minimize the impact of these additional charges, it is imperative to keep ancillary service costs as low as possible. The strategy of every converter is to select the submitted bidding curve  $\mathcal{B}_k$  to maximize its profit (34). Given that the number of converters per network node is typically small, converters are aware of their market influence and may strategically misreport costs to increase profits. As such, it is crucial to promote honest cost reporting and discourage strategic bidding.

In this paper, the VCG mechanism [33] is employed to build the market. Under the VCG mechanism, the allocations of

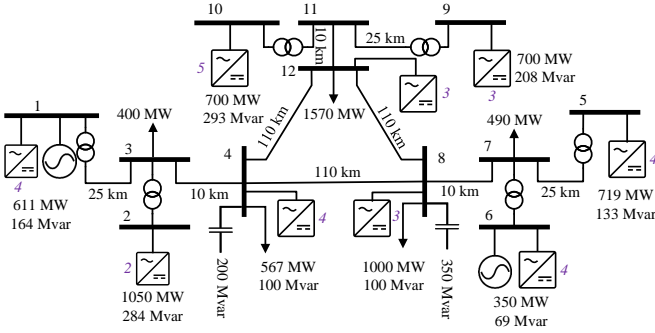


Fig. 5. System topology for the basic test setup. Each node's number of units is indicated by numbers in Italics adjacent to it.

$m_k$  and  $d_k$  are determined by solving the cost minimization problem:

$$\mathbf{m}^*, \mathbf{d}^* = \arg \min \sum_{k \in \mathcal{K}} \mathcal{B}_k(m_k, d_k) \quad (35)$$

The payment  $q_{\hat{k}}$  to converter  $\hat{k}$  is determined as follows:

$$q_{\hat{k}} = \min \sum_{- \hat{k}} \mathcal{B}_k(m_k, d_k) - \sum_{- \hat{k}} \mathcal{B}_k(m_k^*, d_k^*) \quad (36)$$

The first part of the Eq.(36) represents the cost to maintain the stability of the system without the presence of converter  $\hat{k}$ . It takes into account the aggregated cost of all other converters in the system. The second part of the equation represents the summed cost for all other converters with the presence of converter  $\hat{k}$ . The payment is determined by the difference between the two parts, representing the reduction in the overall cost achieved by having converter  $\hat{k}$  participate in the market. Namely, each converter unit gets paid according to the negative externality. For rational generation, the VCG mechanism is proven to satisfy the following properties:

**Proposition 3.** VCG mechanism satisfies the following properties:

- **Efficiency Maximization:** The allocation of inertia and damping coefficients obtained through the VCG mechanism minimizes the total cost required to provide them.
- **Individual Rationality:** The payment made to every converter under the VCG mechanism is non-negative, meaning that each converter receives compensation for its contribution to the system stability.
- **Incentive Compatible:** For each converter, truthfully reporting its cost function (bidding curve) is a dominant strategy.

$$u_k(\mathcal{C}_k, \mathcal{B}_{-k}) \geq u_k(\mathcal{B}_k, \mathcal{B}_{-k}), \forall \mathcal{B}_k, \forall k \quad (37)$$

*Proof.* See appendix.  $\square$

## IV. CASE STUDIES

### A. Setting

A case study was conducted on a 3-area 12-bus test system, as depicted in Fig.5 [9]. For this study, a disturbance of 0.3 pu (equivalent to 300 MW) is introduced to the system. An oscillation mode decay requirement was specified at  $\beta = 0.5$ . The damping ratio for the mode was determined as

$\cos \zeta = 0.12$ , surpassing the grid code's minimum requirement of 0.1 [34] to ensure robustness. RoCoF's threshold was set at  $\varepsilon_{\text{RoCoF}} = 0.5$  Hz/s. Limits for the steady-state frequency deviation and the frequency nadir were established at  $\varepsilon_{\text{sync}} = 0.3$  Hz and  $\varepsilon_{\text{nadir}} = 0.5$  Hz, respectively. For all nodes, we assumed a baseline inertia of  $m_i = 10^{-2}$  pu and a minimum damping of  $d_i = 10^{-2}$  pu. Nodes 1 and 6 each host one synchronous generator, both having a fixed rotational inertia of  $m_k = 2$  s. For each synchronous generator, the turbine dynamic parameters are set as  $r_k^{-1} = 9$  and  $\tau_k = 5$  s, leading to a COI turbine dynamic of  $r^{-1} = 18$  and  $\tau = 5$  s. Coefficients for the empirical inverse nadir function were computed with  $\kappa = 3$ , with specific values determined as  $\Theta_m = 0.1160$ ,  $\Theta_d = 0.9541$ , and  $\Theta = 3.8683$ . Upon analysis, numerical results suggest that the mean approximated error is 1.22% for the range  $(m_{\Sigma}, d_{\Sigma}) \in [5, 60] \times [5, 60]$ .

We consider a high renewable penetration level where the electricity price  $\mathbf{p}$  is expected to vary from 4 to 10 \$/MWh, approximately 20% of the current wholesale market electricity price [35]. The focus is mainly on the power reservation cost. For the cost coefficients, we set  $\mu_{m,k} = \mathbf{p}_k \varepsilon_{\text{RoCoF}}$  and  $\mu_{d,k} = \mathbf{p}_k \varepsilon_{\text{nadir}}$  for each converter  $k$ . Here,  $\mathbf{p}_k$  represents the unit cost related to the electricity price, which is randomly selected in the range of [4, 10]. The quadratic coefficients are set as  $\varrho_{m,k} = \mu_{m,k}/50$  and  $\varrho_{d,k} = \mu_{d,k}/50$  to establish the quadratic cost functions for the converters. We assume multiple converters are located at each node, and the number of converters is shown in Fig.5. Each converter is owned by a different manufacturer. If two converters at the same node submit identical winning bids, they will split the winning bids, and receive an equal distribution of the inertia and damping allocation. All the experiments are implemented using Matlab software on a workstation with an Intel® Core i9-10900K @ 3.70GHz CPU and 128.0 GB of RAM. The aggregation cost optimization problem is solved using the Mosek solver.

### B. Optimization Result

We first analyze the solutions to the market clearing problem. For comparison, we consider two scenarios: one with both small-signal and frequency stability constraints (referred to as 'small-signal + frequency stability'), and the other with only frequency stability constraints (referred to as 'frequency stability'). The latter scenario is a common practice in current research. By comparing the results of these two scenarios, we can assess the impact of incorporating small-signal constraints on system dynamic performance enhancement. The total inertia for both cases amounts to  $\sum_i m_i = 30.0$  s (including the fixed rotational inertia provided by synchronous generators). The total damping for both scenarios is  $\sum_i d_i = 36.0$  pu. When both small-signal and frequency stability are factored in, inertia and damping are distributed more evenly throughout the network. In contrast, when considering frequency stability within the operational constraints alone, some nodes exhibit exceptionally low damping, shown in Fig.6. Ineffectively distributed damping can push the system towards a marginally stable state, possibly triggering intense oscillations. Integration of small-signal constraints acts as a preventive measure against such complications, subsequently supporting system stability.

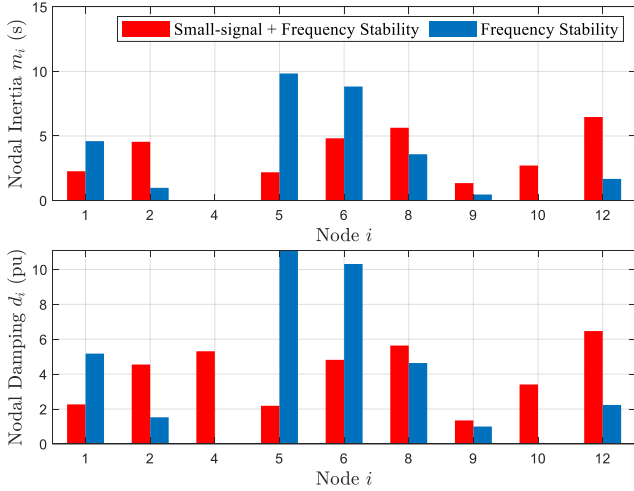


Fig. 6. The allocation of  $m_i$  and  $d_i$  for node  $i$ .

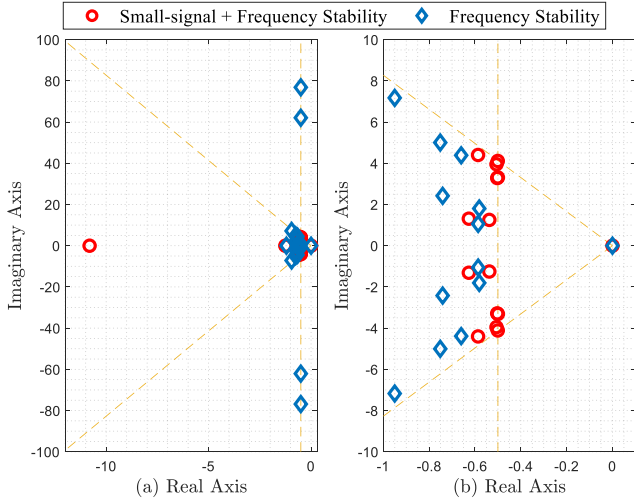


Fig. 7. (a) The eigenvalue maps of the two solutions. (b) The zoomed eigenvalue maps near the origin of the two solutions. The dashed lines represent the boundaries of the desired eigenvalue region. The sufficient constraints presented in Theorem 1 are tight, with 4 pairs of complex eigenvalues are positioned at the constrained boundary.

The eigenvalue maps of the two solutions are depicted in Fig.7. The dashed lines represent the boundaries of the desired eigenvalue region set in the optimization problem ( $\lambda \leq \beta$  and  $\sin \zeta \cdot \text{Re}(\lambda) + \cos \zeta \cdot \text{Im}(\lambda) \leq 0$ ). In Fig.7(a), it can be observed that the 'frequency stability' solution yields two pairs of eigenvalues with very poor damping performance, as the imaginary part of these modes is over 100 times their real part. In contrast, Fig.7(b) demonstrates that the small-signal constraint is effective in constraining the eigenvalues within the desired region. The 'small-signal + frequency stability' solution successfully keeps all the eigenvalues in the desired region. These results confirm the effectiveness of incorporating small-signal constraints in the optimization problem, ensuring better damping performance and overall system stability.

The impact of poor damping modes can also be observed in the time-domain response. Fig.8 (a-b), (c-d) show the frequency deviations in the time domain when the disturbance

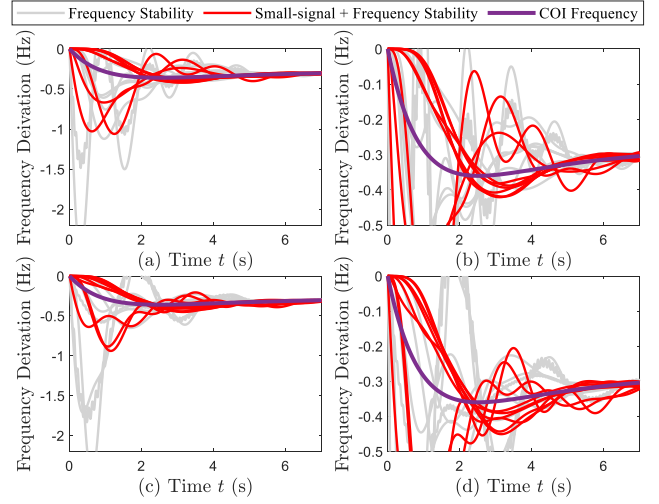


Fig. 8. The nodal frequency response (a) and its zoomed version in (b) when the disturbance happens at node 2. The nodal frequency response (c) and its zoomed version in (d) when the disturbance happens at node 12.

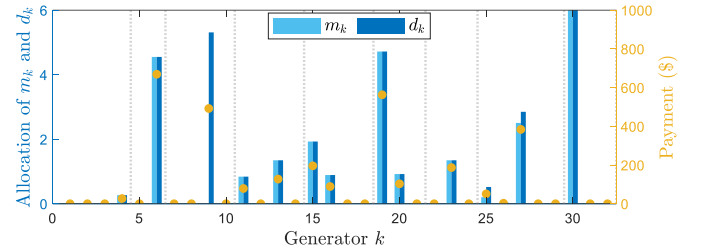


Fig. 9. The allocations of  $m_k$  and  $d_k$ , together with the market payment in the basic case. The dashed gray line indicates the node that the converter belongs to.

occurs at nodes 2 and 12, respectively. In both cases, it is evident that the overall oscillation amplitude is reduced, and the differences between individual nodal frequency and the global frequency are relatively smaller. This confirms the effectiveness of incorporating both global frequency stability and small-signal stability constraints in maintaining nodal frequency transient performance.

### C. Market Clearing Result

The results of the oscillation damping market clearing are analyzed next. The allocations of  $m_k$  and  $d_k$ , along with the market payments, are shown in Fig.9. Under the VCG mechanism, the payment may not always be proportional to the allocation, as it depends on the alternatives available to each converter.

We assess the truthfulness properties of the VCG mechanism by focusing on converter 15 as an example. Assuming it misrepresents its real cost as  $\mu_{m,k} = p'_k \epsilon_{\text{RoCoF}}$ , where  $p'_k \in [3, 11]$  \$/MWh, the other cost coefficients are modified accordingly. We then compute the profits under varying bids, as shown in Fig.10. The findings suggest that the highest profit for converter 15 is achieved when it places a bid equivalent to its actual cost. If it attempts to place high bids, it wouldn't secure as many bids as it would when bidding truthfully, thus



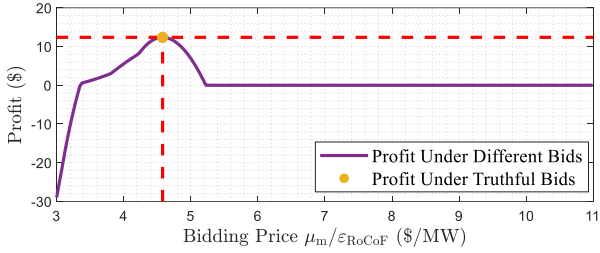


Fig. 10. Profits under different bids for converter 15.

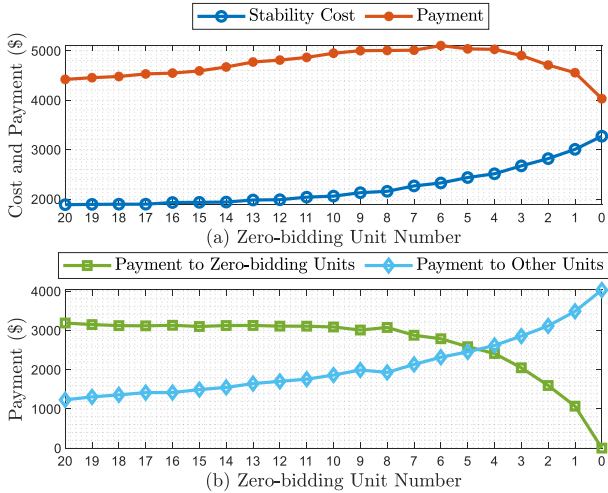


Fig. 11. (a) Stability cost and payments under different proportions of zero-bidding converters. (b) Payments to different types of converters under different proportions of zero-bidding rotating converters.

its total profit diminishes. Conversely, if it attempts to place low bids to win additional bids, the payment wouldn't offset the costs, leading to a decrease in its total profit.

We investigate the impact of zero-bidding by wind generators, which can provide inertia at almost zero cost due to their rotating machinery. Fig.11 displays the market-clearing results under varying proportions of converters that submit zero inertia bidding costs. In each scenario, a total of 0 to 20 units are randomly chosen to submit zero-bidding for inertia. For each case, 100 random samples are generated to mitigate the influence of randomness. From Fig.11(a), we can see that the stability cost steadily increases as the proportion of converters submitting zero-bids decreases. However, payments to converters decline when there's a very low proportion of zero-bidding converters. This is because the VCG mechanism calculates payments based on each converter's externality. If these zero-bidding converters do not participate in the market, the stability cost will sharply increase. As a result, the payments to them will also be very high. This trend can also be observed in Fig.11(b), where the decline in payments follows the drop in payments to zero-bidding converters.

The total payment to converters is around 5000 \$. It is worth noting that the payment is equivalent to 500 MWh of electricity if the electricity price is accounted as 10 \$/MWh. In comparison, the electricity traded in energy markets for the case system under this case is around  $4 \times 10^3$  MWh. Hence,

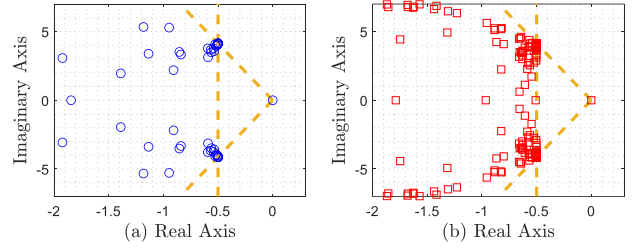


Fig. 12. (a) The eigenvalue maps near the origin for the 500-bus power system test case. (b) The eigenvalue maps near the origin for the 2000-bus power system test case. The dashed lines represent the boundaries of the desired eigenvalue region. The sufficient constraints presented in Theorem 1 are tight.

establishing the market will only incur about 12.5% extra cost. These results have the following positive implications:

- 1) For system operators, they do not need to worry about the payment becoming extremely high when there are large numbers of static converters in the system, as the VCG mechanism ensures fair compensation based on each converter's externality.
- 2) For converters, the market allows them to gain extra revenue by providing appropriate inertia and damping, incentivizing them to contribute to system stability.

#### D. Computational Efficiency

The whole market clearing problem is further tested on larger power system test cases: a 500-bus power system test case in South Carolina, US, and a 2000-bus power system test case in Texas, US. The detailed data used for these test cases can be found in the relevant literature [36]. It is worth noting that the market clearing problem for these larger systems can be efficiently solved. Specifically, the 500-bus power system test case takes only 1.15 seconds to solve, while the 2000-bus power system test case takes 3.33 seconds to solve. These computational times demonstrate that the whole model can be seamlessly integrated into the market operation with reasonable computational efficiency.

Fig.12 displays the eigenvalue maps near the origin for the larger power system test cases. The plots illustrate that the constraints imposed on the eigenvalues are indeed binding and have a significant impact. This successful implementation on larger power system test cases highlights the scalability and practical applicability of the proposed approach. It shows that the market mechanism can handle complex and large-scale power systems, making it a promising solution for real-world power system stability and ancillary service management.

## V. CONCLUSION

This paper presents the establishment of a joint oscillation damping and inertia provision service and formulates a convex cost minimization model to ensure both system small-signal stability and frequency stability. The case studies demonstrate that implementing this service via markets does not incur significant additional costs but is effective in mitigating oscillations.

To extend the research, further work can explore incorporating additional types of oscillation damping services, including oscillation caused by machine-control interactions. This will require considering faster control loops, such as inner voltage control loops and current control loops, and obtaining more detailed control loop parameters. Additionally, as power electronics continue to present new stability challenges, the development of more stability ancillary services could be explored. An interesting question for future investigation is whether a unified stability service market could be developed. Such a market would bring together different stability services to address a wide range of stability challenges in a more comprehensive manner.

## REFERENCES

- [1] U. Markovic, O. Stanojev, P. Aristidou, E. Vrettos, D. Callaway, and G. Hug, "Understanding small-signal stability of low-inertia systems," *IEEE Transactions on Power Systems*, vol. 36, no. 5, pp. 3997–4017, 2021.
- [2] F. Milano, F. Dörfler, G. Hug, D. J. Hill, and G. Verbič, "Foundations and challenges of low-inertia systems (invited paper)," in *2018 Power Systems Computation Conference (PSCC)*, 2018, pp. 1–25.
- [3] L. Xiong, X. Liu, Y. Liu, and F. Zhuo, "Modeling and stability issues of voltage-source converter-dominated power systems: A review," *CSEE Journal of Power and Energy Systems*, vol. 8, no. 6, pp. 1530–1549, 2020.
- [4] W. He, X. Yuan, and J. Hu, "Inertia provision and estimation of PLL-Based DFIG wind turbines," *IEEE Transactions on Power Systems*, vol. 32, no. 1, pp. 510–521, 2017.
- [5] A. Tayyebi, D. Groß, A. Anta, F. Kupzog, and F. Dörfler, "Frequency stability of synchronous machines and grid-forming power converters," *IEEE Journal of Emerging and Selected Topics in Power Electronics*, vol. 8, no. 2, pp. 1004–1018, 2020.
- [6] D. Groß, S. Bolognani, B. K. Poolla, and F. Dörfler, "Increasing the resilience of low-inertia power systems by virtual inertia and damping," in *Proceedings of IREP'2017 Symposium*. International Institute of Research and Education in Power System Dynamics, 2017, p. 64.
- [7] B. Wang and K. Sun, "Formulation and characterization of power system electromechanical oscillations," *IEEE Transactions on Power Systems*, vol. 31, no. 6, pp. 5082–5093, 2016.
- [8] T. S. Borsche, T. Liu, and D. J. Hill, "Effects of rotational inertia on power system damping and frequency transients," in *2015 54th IEEE conference on decision and control (CDC)*. IEEE, 2015, pp. 5940–5946.
- [9] B. K. Poolla, S. Bolognani, and F. Dörfler, "Optimal placement of virtual inertia in power grids," *IEEE Transactions on Automatic Control*, vol. 62, no. 12, pp. 6209–6220, 2017.
- [10] Y. Chen, F. Pan, F. Qiu, A. S. Xavier, T. Zheng, M. Marwali, B. Knueven, Y. Guan, P. B. Luh, and L. Wu, "Security-constrained unit commitment for electricity market: Modeling, solution methods, and future challenges," *IEEE Transactions on Power Systems*, vol. Early Access, 2022.
- [11] D. Gan, R. J. Thomas, and R. D. Zimmerman, "Stability-constrained optimal power flow," *IEEE Transactions on Power Systems*, vol. 15, no. 2, pp. 535–540, 2000.
- [12] Y. Xu, Z. Y. Dong, Z. Xu, R. Zhang, and K. P. Wong, "Power system transient stability-constrained optimal power flow: A comprehensive review," in *2012 IEEE Power and Energy Society General Meeting*, ser. 2012 IEEE Power and Energy Society General Meeting. IEEE, 2012, pp. 1–7.
- [13] B. Cui and X. A. Sun, "A new voltage stability-constrained optimal power-flow model: Sufficient condition, SOCP representation, and relaxation," *IEEE Transactions on Power Systems*, vol. 33, no. 5, pp. 5092–5102, 2018.
- [14] R. Zárate-Miñano, F. Milano, and A. J. Conejo, "An OPF methodology to ensure small-signal stability," *IEEE Transactions on Power Systems*, vol. 26, no. 3, pp. 1050–1061, 2010.
- [15] L. Badesa, F. Teng, and G. Strbac, "Simultaneous scheduling of multiple frequency services in stochastic unit commitment," *IEEE Transactions on Power Systems*, vol. 34, no. 5, pp. 3858–3868, 2019.
- [16] B. K. Poolla, D. Groß, and F. Dörfler, "Placement and implementation of grid-forming and grid-following virtual inertia and fast frequency response," *IEEE Transactions on Power Systems*, vol. 34, no. 4, pp. 3035–3046, 2019.
- [17] B. K. Poolla, S. Bolognani, N. Li, and F. Dörfler, "A market mechanism for virtual inertia," *IEEE Transactions on Smart Grid*, vol. 11, no. 4, pp. 3570–3579, 2020.
- [18] Z. Liang, R. Mieth, and Y. Dvorkin, "Inertia pricing in stochastic electricity markets," *IEEE Transactions on Power Systems*, vol. 38, no. 3, pp. 2071–2084, 2022.
- [19] A. Sajadi, R. W. Kenyon, and B.-M. Hodge, "Synchronization in electric power networks with inherent heterogeneity up to 100% inverter-based renewable generation," *Nature communications*, vol. 13, no. 1, p. 2490, 2022.
- [20] Y. Li and Y. Gu, "Whole-system first-swing stability of inverter-based inertia-free power systems," *arXiv*, p. 2207.03292, 2023.
- [21] C. Yang, L. Huang, H. Xin, and P. Ju, "Placing grid-forming converters to enhance small signal stability of PLL-integrated power systems," *IEEE Transactions on Power Systems*, vol. 36, no. 4, pp. 3563–3573, 2020.
- [22] A. Venkatraman, U. Markovic, D. Shchetinin, E. Vrettos, P. Aristidou, and G. Hug, "Improving dynamic performance of low-inertia systems through eigensensitivity optimization," *IEEE Transactions on Power Systems*, vol. 36, no. 5, pp. 4075–4088, 2021.
- [23] L. Yang, Z. Xu, J. Østergaard, Z. Y. Dong, K. P. Wong, and X. Ma, "Oscillatory stability and eigenvalue sensitivity analysis of a dfig wind turbine system," *IEEE Transactions on Energy Conversion*, vol. 26, no. 1, pp. 328–339, 2011.
- [24] L. Guo, C. Zhao, and S. H. Low, "Graph laplacian spectrum and primary frequency regulation," in *2018 IEEE Conference on Decision and Control (CDC)*. IEEE, 2018, pp. 158–165.
- [25] Y. Jiang, R. Pates, and E. Mallada, "Dynamic droop control in low-inertia power systems," *IEEE Transactions on Automatic Control*, vol. 66, no. 8, pp. 3518–3533, 2020.
- [26] M. Tuo and X. Li, "Security-constrained unit commitment considering locational frequency stability in low-inertia power grids," *IEEE Transactions on Power Systems*, vol. Early Access, 2022.
- [27] F. Dörfler and F. Bullo, "Kron reduction of graphs with applications to electrical networks," *IEEE Transactions on Circuits and Systems I: Regular Papers*, vol. 60, no. 1, pp. 150–163, 2012.
- [28] F. Tisseur and K. Meerbergen, "The quadratic eigenvalue problem," *SIAM review*, vol. 43, no. 2, pp. 235–286, 2001.
- [29] M. Chilali, P. Gahinet, and P. Apkarian, "Robust pole placement in LMI regions," *IEEE transactions on Automatic Control*, vol. 44, no. 12, pp. 2257–2270, 1999.
- [30] C. Scherer and S. Weiland, "Linear matrix inequalities in control," *Lecture Notes, Dutch Institute for Systems and Control, Delft, The Netherlands*, vol. 3, no. 2, 2000.
- [31] F. Paganini and E. Mallada, "Global analysis of synchronization performance for power systems: Bridging the theory-practice gap," *IEEE Transactions on Automatic Control*, vol. 65, no. 7, pp. 3007–3022, 2020.
- [32] S. S. Guggilam, C. Zhao, E. Dall'Anese, Y. C. Chen, and S. V. Dhople, "Optimizing DER participation in inertial and primary-frequency response," *IEEE Transactions on Power Systems*, vol. 33, no. 5, pp. 5194–5205, 2018.
- [33] Y. Xu and S. H. Low, "An efficient and incentive compatible mechanism for wholesale electricity markets," *IEEE Transactions on Smart Grid*, vol. 8, no. 1, pp. 128–138, 2015.
- [34] Western Power, "Power system stability requirements guideline," 2021, <https://www.westernpower.com.au/media/4981/power-system-stability-requirements-guideline-20210511.pdf>, Last accessed on 2021-05-11.
- [35] U.S. Energy Information Administration, "Electricity monthly update," 2023, <https://www.eia.gov/electricity/monthly/update/wholesale-markets.php>.
- [36] A. B. Birchfield, T. Xu, K. M. Gegner, K. S. Shetye, and T. J. Overbye, "Grid structural characteristics as validation criteria for synthetic networks," *IEEE Transactions on power systems*, vol. 32, no. 4, pp. 3258–3265, 2016.

## PROOF FOR LEMMA 1

*Proof.* Consider the following quadratic eigenvalue problem:

$$\lambda^2 \mathbf{M}\nu + \lambda \mathbf{D}\nu + \mathbf{L}\nu = \mathbf{0} \quad (38)$$

Since  $\mathbf{L}$  has an eigenvalue of 0 with the eigenvector  $\mathbf{1}$ , we have  $\lambda = 0$  and  $\boldsymbol{\nu} = \mathbf{1}$  as one of the solutions to Eq.(38).

Now, let  $\boldsymbol{\xi}$  and  $\boldsymbol{\nu}$  be the eigenvector and eigenvalue of the matrix  $\mathbf{A}$  such that:

$$\boldsymbol{\xi} = \lambda \boldsymbol{\nu}, \quad -\mathbf{L}\boldsymbol{\nu} - \mathbf{D}\boldsymbol{\xi} = \lambda \mathbf{M}\boldsymbol{\xi} \quad (39)$$

Hence,  $\lambda = 0$  and  $[\boldsymbol{\nu}^\top \boldsymbol{\xi}^\top]^\top = [\mathbf{1}^\top \mathbf{0}^\top]^\top$  are one of the solution to Eq.(39).  $\square$

#### PROOF FOR PROPOSITION 1

We will employ the subsequent definitions and lemmas. The dimension will be represented as  $N$ .

*Definition 1* (Orthogonal Complement Subspace  $\mathbb{I}_\perp$ ). The orthogonal complement subspace of  $\mathbf{1}$  in  $\mathbb{R}^N$  is denoted by  $\mathbb{I}_\perp = \{\mathbf{x} \in \mathbb{R}^N | \mathbf{1}^\top \mathbf{x} = 0\}$ .

*Lemma 4* (Orthogonality of Eigenvectors for Symmetric Matrices). Given a real symmetric matrix  $\mathbf{A}$ , the eigenvectors associated with different eigenvalues are orthogonal.

*Proof.* Consider a symmetric real matrix  $\mathbf{A}$  and suppose  $\sigma_1$  and  $\sigma_2$  are two distinct eigenvalues of  $\mathbf{A}$ , with corresponding eigenvectors  $\mathbf{y}_1$  and  $\mathbf{y}_2$ . By definition of an eigenvector and eigenvalue, we have:

$$\mathbf{A}\mathbf{y}_1 = \sigma_1 \mathbf{y}_1, \quad \mathbf{A}\mathbf{y}_2 = \sigma_2 \mathbf{y}_2 \quad (40)$$

Let's take the dot product of the first equation with  $\mathbf{y}_2$ :

$$\mathbf{y}_2^\top \mathbf{A}\mathbf{y}_1 = \sigma_1 \mathbf{y}_2^\top \mathbf{y}_1$$

We can rewrite the left-hand side as:

$$\mathbf{y}_2^\top \mathbf{A}\mathbf{y}_1 = \mathbf{y}_1^\top \mathbf{A}^\top \mathbf{y}_2$$

Since  $\mathbf{A}$  is symmetric,  $\mathbf{A}^\top = \mathbf{A}$ . So,  $\mathbf{y}_1^\top \mathbf{A}\mathbf{y}_2 = \mathbf{y}_1^\top \sigma_2 \mathbf{y}_2 = \sigma_2 \mathbf{y}_1^\top \mathbf{y}_2$ . Combining the two equations, we get:

$$\sigma_1 \mathbf{y}_2^\top \mathbf{y}_1 = \sigma_2 \mathbf{y}_1^\top \mathbf{y}_2$$

Rearranging:

$$\sigma_1 \mathbf{y}_2^\top \mathbf{y}_1 - \sigma_2 \mathbf{y}_1^\top \mathbf{y}_2 = 0$$

Since  $\sigma_1$  and  $\sigma_2$  are distinct and  $\mathbf{y}_2^\top \mathbf{y}_1 = \mathbf{y}_1^\top \mathbf{y}_2$ , the only way the above equation can hold true is if  $\mathbf{y}_2^\top \mathbf{y}_1 = 0$ , which means the vectors  $\mathbf{y}_1$  and  $\mathbf{y}_2$  are orthogonal.  $\square$

*Lemma 5* (Subspace Positive Semi-definiteness). If  $\mathbf{L} - \beta \mathbf{D} + \beta^2 \mathbf{M} + v \mathbf{1}\mathbf{1}^\top \succcurlyeq 0$ , then the matrix  $\mathbf{L} - \beta \mathbf{D} + \beta^2 \mathbf{M}$  is positive semi-definite on  $\mathbb{I}_\perp$ .

*Proof.* Because  $\mathbf{L} - \beta \mathbf{D} + \beta^2 \mathbf{M} + v \mathbf{1}\mathbf{1}^\top \succcurlyeq 0$ :

$$\mathbf{x}^\top (\mathbf{L} - \beta \mathbf{D} + \beta^2 \mathbf{M} + v \mathbf{1}\mathbf{1}^\top) \mathbf{x} \geq 0$$

for all  $\mathbf{x} \in \mathbb{I}_\perp$ . Besides, due to  $\mathbf{1}^\top \mathbf{x} = 0$ , the equation above suggests:

$$\mathbf{x}^\top (\mathbf{L} - \beta \mathbf{D} + \beta^2 \mathbf{M}) \mathbf{x} \geq 0$$

for all  $\mathbf{x} \in \mathbb{I}_\perp$ .  $\square$

*Lemma 6* (Eigenvalues of Subspace Positive Semi-definite Matrix). If a real symmetric matrix  $\mathbf{A}$  is positive definite  $\mathbf{A} \succ 0$  on  $\mathbb{I}_\perp$ , then  $\mathbf{A}$  possesses at most one eigenvalue  $\leq 0$ .

*Proof.* We first prove that there is at most one 0 eigenvalue:

Suppose a vector  $\mathbf{x} \in \mathbb{I}_\perp$  is the solution to  $\mathbf{A}\mathbf{x} = \mathbf{0}$ , which leads to  $\mathbf{x}^\top \mathbf{A}\mathbf{x} = 0$ , which is a contradiction with  $\mathbf{A} \succ 0$  on  $\mathbb{I}_\perp$ . Consequently, all the vectors  $\mathbf{x} \in \mathbb{I}_\perp$  cannot lie in the null space of  $\mathbf{A}$ . The dimension of the null space for  $\mathbf{A}$  must be less or equal to 1:  $\dim(\text{null}(\mathbf{A})) \leq N - \dim(\mathbb{I}_\perp) = 1$ . By the rank-nullity relationship, we know the rank of  $\text{rank}(\mathbf{A}) = N - \dim(\text{null}(\mathbf{A})) \geq N - 1$ , which indicates there at least  $N - 1$  non-zero eigenvalues.

Next, we prove there cannot be multiple non-positive eigenvalues:

By contradiction, suppose there are two different eigenvalues  $\sigma_1 \leq 0$  and  $\sigma_2 \leq 0$ , whose eigenvectors are  $\mathbf{y}_1$  and  $\mathbf{y}_2$ , respectively. Given that  $\text{rank}(\mathbf{A}) \geq N - 1$ ,  $\sigma_1$  and  $\sigma_2$  cannot be 0 simultaneously. Since  $\mathbf{A}$  is a real symmetric matrix, according to lemma 4,  $\mathbf{y}_1 \perp \mathbf{y}_2$ . Because of the linear independence of  $\mathbf{y}_1$  and  $\mathbf{y}_2$ , their span has at least a dimension of 2. We have  $\text{span}\{\mathbf{y}_1, \mathbf{y}_2\} \cap \mathbb{I}_\perp \neq \emptyset$ .

Thereby, there is a nonzero real vector  $\mathbf{z} \in \text{span}\{\mathbf{y}_1, \mathbf{y}_2\}$  such that  $\mathbf{z} \in \mathbb{I}_\perp$ . Let  $\mathbf{z} = a\mathbf{y}_1 + b\mathbf{y}_2$  where at least one of  $a, b$  is not zero. We have:

$$\begin{aligned} \mathbf{z}^\top \mathbf{A}\mathbf{z} &= (a\mathbf{y}_1 + b\mathbf{y}_2)^\top \mathbf{A}(a\mathbf{y}_1 + b\mathbf{y}_2) \\ &= a^2 \mathbf{y}_1^\top \mathbf{A}\mathbf{y}_1 + ab \mathbf{y}_1^\top \mathbf{A}\mathbf{y}_2 + ab \mathbf{y}_2^\top \mathbf{A}\mathbf{y}_1 + b^2 \mathbf{y}_2^\top \mathbf{A}\mathbf{y}_2 \\ &= a^2 \sigma_1 \mathbf{y}_1^\top \mathbf{y}_1 + ab \sigma_2 \mathbf{y}_1^\top \mathbf{y}_2 + ab \sigma_1 \mathbf{y}_2^\top \mathbf{y}_1 + b^2 \sigma_2 \mathbf{y}_2^\top \mathbf{y}_2 \\ &= \sigma_1 a^2 \|\mathbf{y}_1\|^2 + \sigma_2 b^2 \|\mathbf{y}_2\|^2 \leq 0 \end{aligned} \quad (41)$$

which leads to a contradiction to the condition of  $\mathbf{x}^\top \mathbf{A}\mathbf{x} > 0$  for all vectors  $\mathbf{x} \in \mathbb{I}_\perp$ .  $\square$

Now we are ready to prove the proposition 1.

*Proof.* The shifted eigenvalue solution problem is represented as follows:

$$\hat{\lambda}^2 \mathbf{M}\boldsymbol{\nu} + \hat{\lambda} (\mathbf{D} - 2\beta \mathbf{M}) \boldsymbol{\nu} + (\mathbf{L} - \beta \mathbf{D} + \beta^2 \mathbf{M}) \boldsymbol{\nu} = \mathbf{0} \quad (42)$$

The quadratic equation about  $\hat{\lambda}$  can be expressed as:

$$\begin{aligned} \hat{\lambda}^2 \langle \boldsymbol{\nu}, \mathbf{M}\boldsymbol{\nu} \rangle + \hat{\lambda} \langle \boldsymbol{\nu}, (\mathbf{D} - 2\beta \mathbf{M}) \boldsymbol{\nu} \rangle \\ + \langle \boldsymbol{\nu}, (\mathbf{L} - \beta \mathbf{D} + \beta^2 \mathbf{M}) \boldsymbol{\nu} \rangle = 0 \end{aligned} \quad (43)$$

• For complex eigenvalue pairs  $\hat{\lambda}$  and its conjugate  $\hat{\lambda}^*$ , notice the two complex roots of (43) satisfy:

$$\hat{\lambda} + \hat{\lambda}^* = \frac{-\boldsymbol{\nu}^\text{H} (\mathbf{D} - 2\beta \mathbf{M}) \boldsymbol{\nu}}{\boldsymbol{\nu}^\text{H} \mathbf{M} \boldsymbol{\nu}} \quad (44)$$

Thereby, if the first inequality of this proposition is satisfied, we have

$$\hat{\lambda} + \hat{\lambda}^* = \frac{-\boldsymbol{\nu}^\text{H} (\mathbf{D} - 2\beta \mathbf{M}) \boldsymbol{\nu}}{\boldsymbol{\nu}^\text{H} \mathbf{M} \boldsymbol{\nu}} \leq 0 \quad (45)$$

which further indicates the real part of  $\hat{\lambda}$  is less than or equal to zero, and is sufficient to guarantee the complex eigenvalue pairs both have non-positivereal parts.

• For a real eigenvalue  $\hat{\lambda}$  other than eigenvalue  $0 + \beta$ , by contradictions, suppose there is a real eigenvalue larger than zero  $0 < \hat{\lambda} < \beta$  (it must hold that  $\hat{\lambda} < 0 + \beta$  because all

the eigenvalues in the original system strictly lie in the left half plane). Notice (42) can be written as:

$$\underbrace{(\hat{\lambda}^2 \mathbf{M} + \hat{\lambda} (\mathbf{D} - 2\beta \mathbf{M}) + (\mathbf{L} - \beta \mathbf{D} + \beta^2 \mathbf{M}))}_{\mathbf{A}(\hat{\lambda})} \boldsymbol{\nu} = \mathbf{0} \quad (46)$$

Given that  $\hat{\lambda} > 0$ , the following relations hold:  $\hat{\lambda}^2 \mathbf{M} \succ 0$  and  $\hat{\lambda} (\mathbf{D} - 2\beta \mathbf{M}) \succcurlyeq 0$ , which is valid because  $\mathbf{D} - 2\beta \mathbf{M} \succcurlyeq 0$ . Based on Lemma 5, the matrix  $\mathbf{L} - \beta \mathbf{D} + \beta^2 \mathbf{M} \succcurlyeq 0$  is necessarily positive semi-definite over  $\mathbb{I}_\perp$ . When considering the summation of these matrices, the matrix  $\mathbf{A}(\hat{\lambda})$  must be positive definite on  $\mathbb{I}_\perp$ . Referring to Lemma 6, this matrix can have, at most, a single eigenvalue  $\leq 0$ . The other  $N - 1$  eigenvalues must be positive. Our subsequent task is to establish that this eigenvalue must be negative rather than zero.

For  $\mathbf{A}(\hat{\lambda})$ , we have:

$$\mathbf{A}(\hat{\lambda}) = (\hat{\lambda} - \beta)^2 \mathbf{M} + (\hat{\lambda} - \beta) \mathbf{D} + \mathbf{L} \quad (47)$$

$$\preccurlyeq \frac{(\hat{\lambda} - \beta)^2}{2\beta} \mathbf{D} + (\hat{\lambda} - \beta) \mathbf{D} + \mathbf{L} \quad (48)$$

$$= \frac{(\hat{\lambda} - \beta)(\hat{\lambda} + \beta)}{2\beta} \mathbf{D} + \mathbf{L} \quad (49)$$

$$\prec \mathbf{L} \quad (50)$$

where (48) is due to  $\mathbf{D} - 2\beta \mathbf{M} \succcurlyeq 0$ ; (50) is due to  $\hat{\lambda} - \beta < 0$ . The above inequality implies:

$$\mathbf{1}^\top \mathbf{A}(\hat{\lambda}) \mathbf{1} < \mathbf{1}^\top \mathbf{L} \mathbf{1} = 0 \quad (51)$$

From this, it's evident that the matrix  $\mathbf{A}(\hat{\lambda})$  has at least one negative eigenvalue. Consequently, the last eigenvalue must be negative. Given  $\mathbf{A}(\hat{\lambda})$  possesses one negative eigenvalue and  $N - 1$  positive eigenvalues,  $\mathbf{A}(\hat{\lambda})$  is full rank. The only feasible solution to the equation  $\mathbf{A}(\hat{\lambda}) \boldsymbol{\nu} = \mathbf{0}$  is  $\boldsymbol{\nu} = \mathbf{A}(\hat{\lambda})^{-1} \mathbf{0} = \mathbf{0}$ . This presents an inconsistency, implying that no real solution exists in the range  $0 < \hat{\lambda} < \beta$  to solve the quadratic eigenvalue problem.

In summary, all the solutions to  $\hat{\lambda}$  except the  $0 + \beta$  of the shifted eigenvalue problem are in the left half plane. Therefore, the solutions  $\lambda$  except 0 of the original eigenvalue problem are in the plane  $\text{Re}(\lambda) \leq -\beta$ .  $\square$

#### PROOF FOR PROPOSITION 2

*Proof.* For real eigenvalue pairs, the condition is naturally satisfied because the discriminant  $\langle \boldsymbol{\nu}, \mathbf{D} \boldsymbol{\nu} \rangle^2 - 4 \langle \boldsymbol{\nu}, \mathbf{M} \boldsymbol{\nu} \rangle \langle \boldsymbol{\nu}, \mathbf{L} \boldsymbol{\nu} \rangle \geq 0$ .

For complex conjugate eigenvalue pairs  $\lambda$  and  $\lambda^*$ , the necessary and sufficient condition is:

$$\begin{cases} \sin \zeta \cdot (\lambda + \lambda^*) \leq 0 \\ (\sin \zeta)^2 (\lambda + \lambda^*)^2 + (\cos \zeta)^2 (\lambda - \lambda^*)^2 \geq 0 \end{cases} \quad (52)$$

The first inequality is guaranteed because all the eigenvalues except 0 strictly lies in the left-half plane. For the second inequality, by taking

$$(\lambda + \lambda^*)^2 = \left( \frac{-\boldsymbol{\nu}^H \mathbf{D} \boldsymbol{\nu}}{\boldsymbol{\nu}^H \mathbf{M} \boldsymbol{\nu}} \right)^2 \quad (53)$$

$$(\lambda - \lambda^*)^2 = \left( \frac{-\boldsymbol{\nu}^H \mathbf{D} \boldsymbol{\nu}}{\boldsymbol{\nu}^H \mathbf{M} \boldsymbol{\nu}} \right)^2 - 4 \frac{\boldsymbol{\nu}^H \mathbf{L} \boldsymbol{\nu}}{\boldsymbol{\nu}^H \mathbf{M} \boldsymbol{\nu}} \quad (54)$$

into the (52), we can easily get the condition.  $\square$

#### PROOF FOR THEOREM 1

*Proof.* From the first inequality of proposition 1, we have:

$$\langle \boldsymbol{\nu}, \mathbf{D} \boldsymbol{\nu} \rangle \geq 2\beta \langle \boldsymbol{\nu}, \mathbf{M} \boldsymbol{\nu} \rangle > 0 \quad (55)$$

As a result, we obtain:

$$\langle \boldsymbol{\nu}, \mathbf{D} \boldsymbol{\nu} \rangle^2 \geq 2\beta \langle \boldsymbol{\nu}, \mathbf{M} \boldsymbol{\nu} \rangle \langle \boldsymbol{\nu}, \mathbf{D} \boldsymbol{\nu} \rangle \quad (56)$$

Therefore, in order to make the constraint of Proposition 2 hold, the following condition is sufficient:

$$2\beta \langle \boldsymbol{\nu}, \mathbf{M} \boldsymbol{\nu} \rangle \langle \boldsymbol{\nu}, \mathbf{D} \boldsymbol{\nu} \rangle - 4(\cos \zeta)^2 \langle \boldsymbol{\nu}, \mathbf{L} \boldsymbol{\nu} \rangle \langle \boldsymbol{\nu}, \mathbf{M} \boldsymbol{\nu} \rangle \geq 0 \quad (57)$$

Since  $\boldsymbol{\nu}^H \mathbf{M} \boldsymbol{\nu} > 0$ ,  $\beta \mathbf{D} - 2(\cos \zeta)^2 \mathbf{L} \succcurlyeq 0$  implies (57).  $\square$

#### PROOF FOR PROPOSITION 3

*Proof.* Each of the properties is reasoned as follows:

1) Efficiency Maximization: This is obvious because the allocation function aims to minimize the total cost.

2) Individual Rationality: According to the payment function:

$$q_{\hat{k}} = \min \sum_{-\hat{k}} \mathcal{B}_k(m_k, d_k) - \sum_{-\hat{k}} \mathcal{B}_k(m_k^*, d_k^*) \quad (58)$$

If the optimal solution exists for  $\min \sum_{-\hat{k}} \mathcal{B}_k(m_k, d_k)$ , denoted as:

$$\hat{m}_{-\hat{k}}^*, \hat{d}_{-\hat{k}}^* = \min \sum_{-\hat{k}} \mathcal{B}_k(m_k, d_k) \quad (59)$$

Clearly,  $m_{-\hat{k}} = \hat{m}_{-\hat{k}}^*, d_{-\hat{k}} = \hat{d}_{-\hat{k}}^*, m_{\hat{k}} = 0, d_{\hat{k}} = 0$  is one of the feasible solutions to the original cost minimization problem. Thus, the corresponding cost must be larger than the cost of the original optimal solution  $\mathbf{m} = \mathbf{m}^*, \mathbf{d} = \mathbf{d}^*$ .

3) Incentive Compatible: When generator  $\hat{k}$  bid truthfully, the allocation is:

$$\mathbf{m}^*, \mathbf{d}^* = \arg \min \left( \mathcal{C}_{\hat{k}}(m_{\hat{k}}, d_{\hat{k}}) + \sum_{-\hat{k}} \mathcal{B}_k(m_k, d_k) \right) \quad (60)$$

Now, suppose generator  $\hat{k}$  intentionally misreports its cost and bids  $\mathcal{C}'_{\hat{k}}(m_{\hat{k}}, d_{\hat{k}})$ , then the new allocation and payment will be:

$$\begin{aligned} \tilde{\mathbf{m}}^*, \tilde{\mathbf{d}}^* &= \arg \min \left( \mathcal{C}'_{\hat{k}}(m_{\hat{k}}, d_{\hat{k}}) + \sum_{-\hat{k}} \mathcal{B}_k(m_k, d_k) \right) \\ \tilde{q}_{\hat{k}} &= \min \sum_{-\hat{k}} \mathcal{B}_k(m_k, d_k) - \sum_{-\hat{k}} \mathcal{B}_k(\tilde{m}_{\hat{k}}^*, \tilde{d}_{\hat{k}}^*) \end{aligned} \quad (61)$$

The total profit for generator  $\hat{k}$  should be:

$$\begin{aligned} \tilde{u}_{\hat{k}}^* &= \min \sum_{-\hat{k}} \mathcal{B}_k(m_k, d_k) - \\ &\quad \left( \sum_{-\hat{k}} \mathcal{B}_k(\tilde{m}_{\hat{k}}^*, \tilde{d}_{\hat{k}}^*) + \mathcal{C}_{\hat{k}}(\tilde{m}_{\hat{k}}^*, \tilde{d}_{\hat{k}}^*) \right) \end{aligned} \quad (62)$$

where  $\sum_{-\hat{k}} \mathcal{B}_k(\tilde{m}_{\hat{k}}^*, \tilde{d}_{\hat{k}}^*) + \mathcal{C}_{\hat{k}}(\tilde{m}_{\hat{k}}^*, \tilde{d}_{\hat{k}}^*)$  must be larger than  $\sum_{-\hat{k}} \mathcal{B}_k(m_k^*, d_k^*) + \mathcal{C}_{\hat{k}}(m_{\hat{k}}^*, d_{\hat{k}}^*)$  because of (60). Thus, for a rational generator seeking to maximize its profit, its dominant strategy is to submit its true costs.  $\square$